Genesis of Ru_xSe_y Nanoparticles by Pyrolysis of $Ru_4Se_2(CO)_{11}$: A Combined X-ray in Situ and DFT Study

W. Vogel,† P. Kaghazchi,† T. Jacob,† and N. Alonso-Vante*

Fritz-Haber-Institut der Max-Planck-Gesellschaft, Faradayweg 4-6, 14195 Berlin, Germany, and Lab. Electrocatalysis, UMR CNRS 6503, University of Poitiers, 40 Av. Recteur Pineau, F-86022 Poitiers Cedex, France

Received: September 18, 2006; In Final Form: January 6, 2007

The cluster-like Ru_xSe_y ($x \approx 2$, $y \approx 1$) compound can be prepared by simple pyrolysis of the carbonyl complex $Ru_4Se_2(CO)_{11}$ in inert gas. We have observed this process in situ using X-ray diffraction. The clusters exhibit a disordered *hcp*-type structure with an average size of 1.7 nm. Selenium is probably coordinated at the surface of ruthenium nanoparticles. Up to 430 °C, these nanoparticles are stable in an inert ambient, except for a certain growth in size. Above this temperature, the system splits into two phases: *hcp*-type ruthenium particles, which are probably free of Se, and a ruthenium-diselenide phase: $RuSe_2$. Using density functional theory (DFT), we studied the surface structure of $RuSe_2$ and found a preference for Se-rich surfaces. Transferring to the nanoparticles, this might correspond to the picture of a Ru core and either a Ru_xSe_y- or a pure Se shell (adsorbate layer).

Introduction

The electrocatalytic activity toward the oxygen reduction reaction (ORR) in acid medium, as well as the selectivity in the presence of methanol, has been studied on ruthenium chalcogenide-like clusters.[1−3] We have shown that the cluster-like compound Ru_xSe_y prepared from the precursor $Ru_3(CO)_{12}$ and addition of selenium in xylene or 1,2-dichlorobenzene has superior properties against pure Ru_x clusters with respect to its structural stability and its resistance to oxidation in the presence of oxygen in the gas phase.[4] Albeit ruthenium and selenium are immiscible in the bulk phase but only form the single compound $RuSe_2$; no separate Se-containing phase has been observed during the cluster formation, and the electronic state of Se in our Ru_xSe_y cluster compound is still an open question. Using the same chemical synthesis route, other authors prepared similar compounds with a consecutive sintering in selenium atmosphere.[5] However, the descriptive stoichiometry is most probably the result of an incomplete reaction time of pyrolysis of the chemicals and makes the comprehension of the electrocatalysis versus materials science research difficult. A review summarizing the use of transition-metal carbonyl complexes as chemical precursors for tailoring catalyst materials for anodes and cathodes has been reported recently.[6] In this work, to clarify the fate of the selenium during cluster formation, we have performed an in situ X-ray diffraction study, starting with the heteronuclear carbonyl complex $Ru_4Se_2(CO)_{11}$ that forms during the Ru_xSe_y cluster preparation,[7−9] by pyrolytical decomposition of this compound in an inert gas ambient. The intention of this study is to get more insight into the structure of the intermediates and mechanisms of their formation.

Experimental Section

Synthesis of $Ru_4Se_2(CO)_{11}$ in 1,2-Dicholorobenzene. The synthesis of $Ru_4Se_2(CO)_{11}$ occurs during the first 60 min of the reaction of 0.15 mmol of $Ru_3(CO)_{12}$ (99% assay, Alfa Aesar) with 2.3 mmol of selenium (Alpha no. 36208, <325 Mesh) in 100 mL of organic solvent. As reported previously,[10,11] the synthesis completion (20 h reaction time) leads to the formation of an Ru_xSe_y nanostructured powder. However, a selective production of $Ru_4Se_2(CO)_{11}$ takes place in 1,2-dichlorobenzene (Merck).[11,12] The reaction is conducted in an inert atmosphere of nitrogen under refluxing conditions. The synthesis temperature was determined by the boiling point of the solvent at 180 °C. The complex in the solution was recovered and cooled down after a reaction time of 60 min to $T < 0$ °C to stop the reaction. The solvent was evaporated in a rota-vapor at 70 °C and 13 mbar. The resulting solid was dissolved in dichloromethane. Thin-layer chromatography was applied to separate the complex from unreacted $Ru_3(CO)_{12}$, which was very little. This separation was carried out in a mixture of ethyl ether and ethyl acetate (50:50) using a 1-mm-thick immobilized silica layer on a glass plate. The complex did not migrate and was extracted with dichloromethane and dried. The purity of the complexes thus separated could be controlled by high-performance liquid chromatography on column. By comparing the XRD diffraction measurements with the ICSD data (collection code 73582), the structure of $Ru_4Se_2(CO)_{11}$ was identified, see Figure 1. This synthesis route is particularly very facile in comparison to a synthesis reported some time ago by Layer et al.[13] using $Ru_3(CO)_{12}$ and PhSeSePh in a closed ampule under vacuum at 185 °C for 19 h.

X-ray Diffraction and Debye Function Analysis (DFA). X-ray patterns were obtained with a Guinier powder diffractometer (HUBER), set to the 45° transmission position. A Johansson-type Ge monochromator produces a focused monochromatic Cu $K_{\alpha 1}$ primary beam ($\lambda = 1.5406$ Å). Structural changes in different ambients at elevated temperatures can be studied with a specially designed in situ cell attached to the goniometer.[14,15] The powder samples were pressed slightly to pellets $8 \times 15.5 \times 0.1$ mm^3 in size. These pellets were mechanically unstable and were accordingly fixed tightly, but

* Corresponding author. E-mail: Nicolas.alonso.vante@univ-poitiers.fr. University of Poitiers. Tel.: +3354945-3625; fax: +3354945-3580.
† Fritz-Haber-Institut.

10.1021/jp066091p CCC: $37.00
Published on Web 02/21/2007

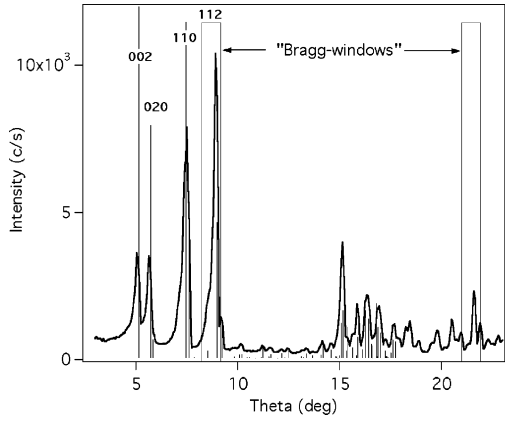

Figure 1. XRD pattern of $Ru_4Se_2(CO)_{11}$. The vertical bars show the structure factors of the carbonyl complex. The boxes indicate the Bragg windows of the open slit position (see the text).

not gastight, between two 0.1 mm beryllium plates before inserting them into the sample holder. In the so-called open slit (OS) mode, the counter slit was set stationary to one or two prominent peaks of the sample. In this mode, time-resolved in situ studies of particle growth or oxide formation are possible. Some angular scans were performed ex situ. In this case, the samples were fixed between two 0.003 mm polyethylene foils and immediately measured in ambient conditions. The background-corrected patterns were subjected to the usual angular correction for absorption, polarization, and geometrical factors and plotted versus the reciprocal scattering length $b = 2 \sin(\theta)/\lambda$.

DFT Calculations. To study the stability of all low-index $RuSe_2$ surfaces, density functional theory (DFT) pseudopotential slab calculations were preformed using the SeqQuest code.[16,17] Throughout the calculations, the PBE[18] generalized gradient approximation (GGA) exchange-correlation functional was used together with a standard (nonlocal) norm-conserving pseudopotential[19] invoking a nonlinear core correction.[20] The basis sets were optimized "double-ζ plus polarization" contracted Gaussian functions.

With these calculated parameters, we first studied the bulk properties of $RuSe_2$ in the well-known pyrite structure. The optimized lattice constant of 6.07 Å deviates from the experimental value by only 2.4% and is also in good agreement with all-electron calculations[21] (a_0 = 6.0 Å). In addition, the formation energy gained by forming a unit of $RuSe_2$ bulk out of Ru bulk and Se bulk of 0.41 eV and the bulk modulus of 1.34 Mbar conform to corresponding all-electron calculations of 0.41 eV and 1.36 Mbar, respectively. On the basis of the calculated lattice constant, all low-index $RuSe_2$ surfaces were studied using slabs of at least 17 layers (showing convergence with slab thickness) separated by 20 Å vacuum. In each case, the entire geometry of the system was allowed to freely optimize (to <0.01 eV/Å), resulting in symmetric top and bottom slabs.

Thermodynamic Considerations. To compare the stability of different surfaces, the important quantity is the surface free energy

$$\gamma = \frac{1}{A}[G^{\text{slab}} - N_{\text{Ru}}\mu_{\text{Ru}} - N_{\text{Se}}\mu_{\text{Se}}] \qquad (1)$$

where A is the surface area (in the case of our slab geometries, both the top and bottom layers have to be considered) and G^{slab} is the Gibbs free energy of the slab containing Ru and Se atoms (N_{Ru} and N_{Se}) with the chemical potential μ_{Ru} and μ_{Se} of their corresponding reservoirs. Because in the present work we concentrate on $RuSe_2$ surfaces, we assume that bulk $RuSe_2$ is in equilibrium with both reservoirs, leading to

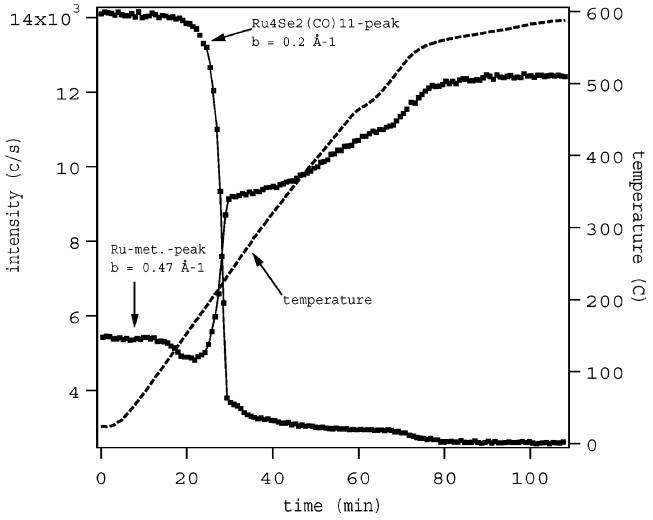

Figure 2. Intensity measured at the 112 peak of carbonyl complex precursor $Ru_4Se_2(CO)_{11}$ and around the strongest peak of *hcp* ruthenium $\theta = 21.4°$ (see the Bragg windows in Figure 2). The XRD measurement was performed in nitrogen under in situ conditions as a function of time and temperature (see the text).

$$\mu^{\text{bulk}}_{\text{RuSe}_2} = \mu_{\text{Ru}} + 2\mu_{\text{Se}} \qquad (2)$$

Using this condition to replace μ_{Se}, eq 1 becomes

$$\gamma = \frac{1}{A}\left[G^{\text{slab}} - \frac{N_{\text{Se}}}{2} g^{\text{bulk}}_{\text{RuSe}_2} + \left(\frac{N_{\text{Se}}}{2} - N_{\text{Ru}}\right)\mu_{\text{Ru}}\right] \qquad (3)$$

where we replaced $\mu^{\text{bulk}}_{\text{RuSe}_2}$ by the Gibbs free energy $g^{\text{bulk}}_{\text{RuSe}_2}$ of the bulk compound. Because in our calculation we only consider solid surfaces, entropy contributions are expected to be small, allowing us to use the DFT total energies instead of G^{slab}. This equation allows us to study the surface phase diagram as a function of μ_{Ru} (in the following we referenced μ_{Ru} to $\mu^{\text{bulk}}_{\text{RuSe}_2}$ by using $\Delta\mu_{\text{Ru}} = \mu_{\text{Ru}} - \mu^{\text{bulk}}_{\text{RuSe}_2}$).

This method allows us to connect the surface with both bulk reservoirs, assuming a continuous exchange of atoms between the surface and both reservoirs. Besides the thermodynamic equilibrium, which can be described by this approach, the actual process of atom diffusion out of or into the particle itself would be very interesting. But especially on nanoparticles there is a large variety of different processes possible (e.g., on different surface planes, near step edges or kinks, or even more importantly at surface defects), which so far extends the capabilities of quantum-mechanical calculations. Corresponding simulations with larger scale methods will be performed in the near future.

In addition, we would like to point out that because thermodynamics is one of the main driving forces during the compound formation or the genesis, respectively, studying the thermodynamic stable $RuSe_2$ surface structures already provides useful insight into the final surface and bulk structures of the compounds.

Results and Discussion

XRD Analysis. Figure 2 shows an open slit measurement (receiving slit width $\Delta\theta = 1°$) of the intensity around the strongest peak of the carbonyl compound $Ru_4Se_2(CO)_{11}$ (upper curve, Bragg window at $b = 0.2$ Å^{-1} ($\theta = 8.6°$) in Figure 1),

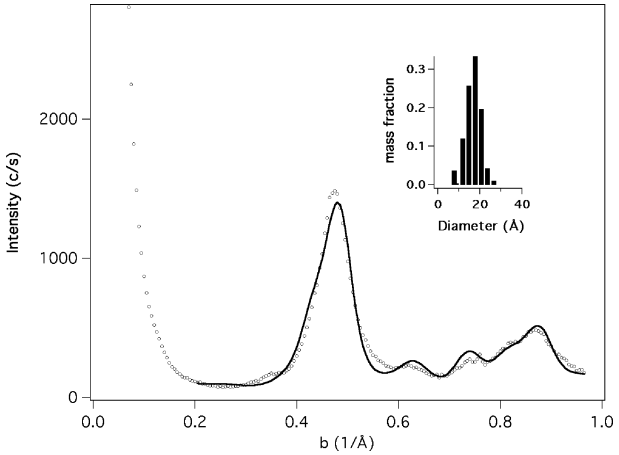

Figure 3. DFA simulation (solid line) of the diffraction pattern of sample Ru_xSe_y after pyrolysis at 220 °C of $Ru_4Se_2(CO)_{11}$. The inset of the figure shows the mass fractions of the *hcp* Ru model particles used for this simulation vs their diameter.

and at the same time the intensity around the diffuse peak expected for nanoscale ruthenium particles (lower curve, Bragg window at $b = 0.47$ Å^{-1} ($\theta = 21.4°$) in Figure 3, and cf. Figure 1). During the measurement, the sample was treated by flowing nitrogen (purity 6.0) or alternatively in helium with a temperature ramp of 8 °C/min or 2 °C/min. It is evident that the crystalline structure of the carbonyl phase breaks down at around 220 °C, which is related to the rapid loss of intensity of the $Ru_4Se_2(CO)_{11}$ peak.

The small further decrease of the intensity at higher temperatures ca. 500 °C can be attributed to growth processes. The simultaneous intensity increase in the second Bragg window relates to the formation of a nanoscale phase of ruthenium.[22] Figure 1 shows the diffraction pattern of the precursor carbonyl[7] compared with the structure factors of the bulk carbonyl as referred to the Joint Committee on Powder Diffraction Standards International Center for Diffraction Data (JCPDS-ICDD) database, while Figure 3 shows the diffraction pattern of the same material taken after pyrolysis in helium was stopped at 220 °C. The solid line in this figure is a simulation calculation using *hcp*-type ruthenium model particles of sizes around 1−3 nm. The related size distribution resulting from the simulation is given in the inset of Figure 3. This data have been achieved by the method of Debye function analysis (DFA) explained elsewhere.[8,9] The result of thermal decomposition in the gas phase is very similar to our earlier investigation of cluster-like compound Ru_xSe_y prepared by the decomposition in dichlorobenzene: *hcp* nanoparticles with an average size of 1.7 nm, an interatomic distance equal to bulk ruthenium, and no indication of a separate Se-containing phase is detected.

When the treatment temperature in He is increased to 430 °C (Figure 4), no dramatic changes are visible in the diffraction pattern, except a narrowing of the *hcp* ruthenium lines due to a certain growth of the particles. The two arrows in the figure inset point to two weak and diffuse peaks assigned to a first formation of very small pyrite-type $RuSe_2$ particles. Figure 5 shows the DFA simulation of the corrected diffraction pattern (beryllium background removed) after final heating in helium at 430 °C for 80 min. The particles have a surprisingly uniform size of 3.1 nm at that stage; see the inset of Figure 5.

After treatment in N_2 at a temperature around 600 °C (cf. Figure 2), the diffraction pattern splits into two phases: a ruthenium phase, probably free of selenium, and the ruthenium diselenide phase ($RuSe_2$). This result is evident from the

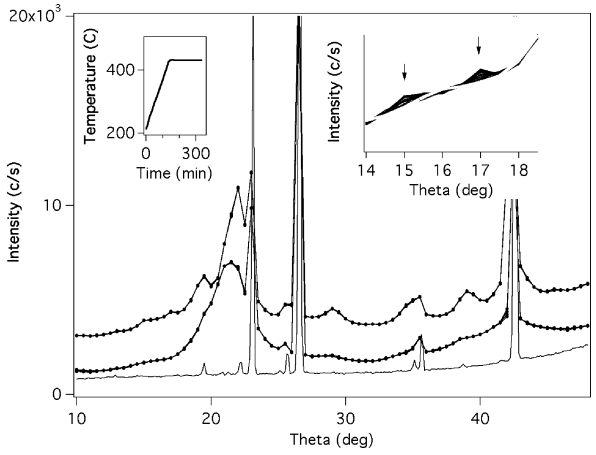

Figure 4. Set of 36 low-resolution in situ θ-scans in helium between 214 and 431 °C. Each scan takes 8 min. The left inset of the figure shows the thermal treatment (ramp rate = 2 °C/min). The figure displays only the first four and the last four scans; the latter are shown with an offset. The intensity plotted as a thin line is the contribution produced by the two beryllium plates of the sample holder. The second inset is a detailed picture in the θ range from 14 to 18°. The grayish curves represent scans at increasing temperature up to 431 °C. The darker curves were taken at a constant temperature of 431 °C. The arrows indicate the development of $RuSe_2$−pyrite peaks 200 and 210 (cf. Figure 6).

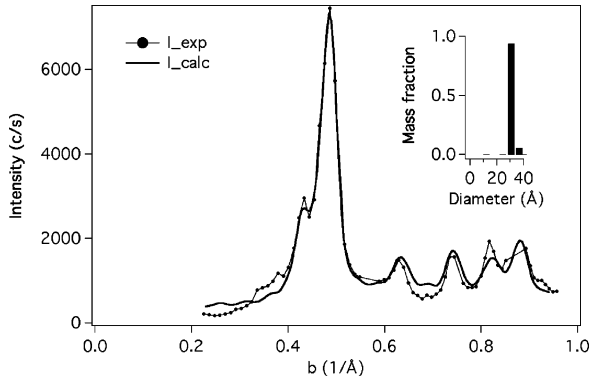

Figure 5. The last four averaged scans of Figure 4 are shown after correction of the background and the application of angular correction factors (dotted curves). The solid line is a DFA simulation of the diffraction pattern using *hcp* ruthenium model clusters. The inset shows the resulting mass fraction vs cluster diameter.

structure factors of both phases that are plotted as vertical bars in Figure 6. The transition into two physically separated phases apparently begins at 430−500 °C, and a second increase of the slope in the OS measurement (Figure 2, Bragg window at $b = 0.47$ Å^{-1}) is indicative of the transition.

Ru_xSe_y Surface Morphology. Studying the structure of realistic Ru_xSe_y nanoparticles usually requires large system sizes and long time scales, which is far out of the range of quantum-mechanical calculations. However, as a first step toward understanding the structure of those compounds we idealized to (semi-)infinitely extended surfaces (length scale) and the thermodynamic equilibrium (time scale). This already allows us to study the preferred surface structure, which due to thermodynamics at least the larger particles try to adopt, for different environmental conditions (given by the Ru-chemical potentials). The structure and composition of smaller particles might also be influenced by so-called quantum-size effects, but this is out of the scope of the present work.

For the surface morphology of Ru/Se nanoparticles, we have to consider two cases:

1. $\mu_{RuSe_2} > \mu_{Ru} + 2\mu_{Se}$: Under this condition, the formation of bulk $RuSe_2$ is thermodynamically unfavorable. Therefore, it

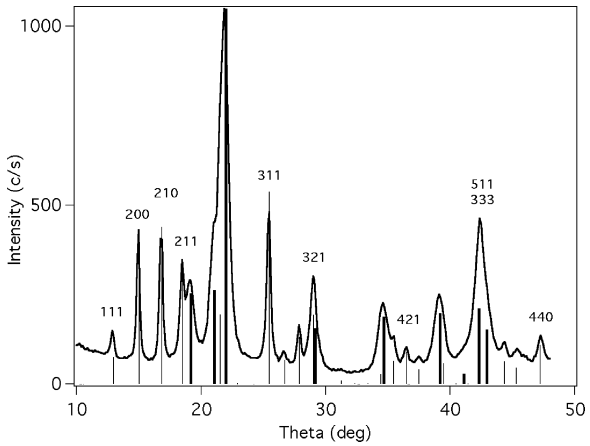

Figure 6. WAXS pattern of Ru_xSe_y after 600 °C treatment. The thick vertical bars show the *hcp* structure of Ru. The presence of the $RuSe_2$−pyrite phase is also evident (thin bars and some Miller indices).

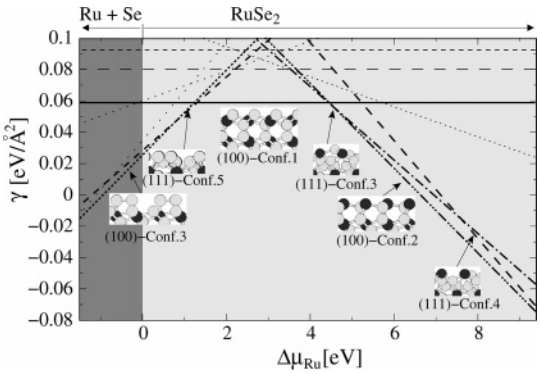

Figure 7. Surface phase diagram of $RuSe_2$ (pyrite-structure) involving all low-index surfaces. For $\Delta\mu_{Ru} = 0$ eV ($\Delta\mu_{Ru}$ is referenced to μ_{RuSe_2}), where the $RuSe_2$ compound is in equilibrium with both reservoirs (Se bulk and Ru bulk), a Se-terminated surface is the most stable thermodynamically. Increasing $\Delta\mu_{Ru}$ leads to a depletion of Se from the surface.

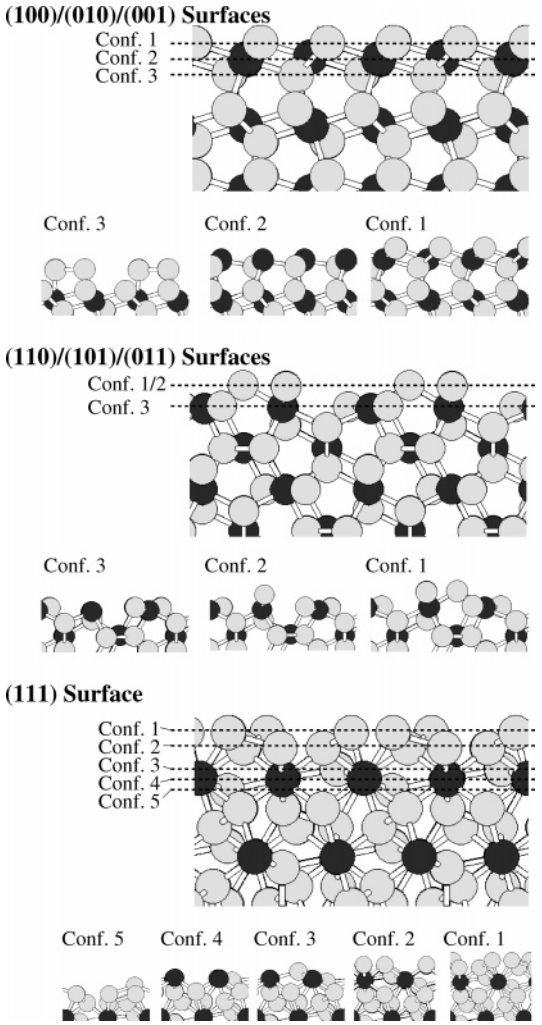

Figure 8. Hard-sphere models of the different surfaces studied to calculate the surface phase diagram (see Figure 7). For each surface, different terminations were possible, leading to the various configurations (geometry optimized structures are shown) shown below each system.

can be assumed that all Se present in a particular Ru_xSe_y particle will be at or near the surface of a pure Ru particle (Ru core). However, besides forming a layer of adsorbed Se on the surface it might also be possible that the Ru core is covered with a thin shell of a certain Ru_xSe_y phase. With regard to the phase diagram shown in Figure 7, this corresponds to the area in which $\Delta\mu_{Ru} < 0$. Compared to the bulk-terminated surface of $RuSe_2$, which would result in a horizontal line in the phase diagram, under those conditions even the pyrite crystal structure seems to prefer a Se-rich surface, which under these conditions might also support the picture of the particle structure, consisting of a Ru core with a selenide phase on the surface. The exact structure will be subject of a forthcoming publication.

2. $\mu_{RuSe_2} \leq \mu_{Ru} + 2\mu_{Se}$: Under this condition, the formation of $RuSe_2$ is thermodynamically favorable. To investigate the preferred surface composition for this case, all low-index surfaces of $RuSe_2$ with different surface terminations were calculated and will be discussed in the following.

The different, nonequivalent surface structures of $RuSe_2$ are shown in Figure 8. With both the (100) and (110) surfaces, three different surface terminations are possible. For $RuSe_2$(100) configurations 1 and 3 are Se-terminated, whereas the latter one shows the stronger changes in the surface structure due to relaxation. This is certainly because of the large amount of Se atoms on the surface, which are not stabilized by the presence of Ru atoms. Similar to $RuSe_2$(110) there are also two Se-terminated surface configurations (1 and 2). However, compared to (100) the surface relaxation for all three configurations is much smaller. The $RuSe_2$(111) surface is more complex. Here we have to distinguish five different surface structures. Starting with configuration 5, which accumulates most Se on the surface, the amount decreases in the following order of configurations: 5−1−2−3, finally leading to the Ru-terminated surface of configuration 4.

On the basis of the DFT-calculated total energies of the various slabs, the surface free energies, which were evaluated with eq 3, are summarized in Figure 7. Because the $RuSe_2$ bulk phase is only stable for $\Delta\mu_{Ru} \geq 0$ eV, in the following we will focus on this condition. At $\Delta\mu_{Ru} = 0$ eV, where both phases (the separated and pyrite phase) are in thermodynamic equilibrium (which is the most interesting condition), we find configuration 5 of $RuSe_2$(111) to be the most stable thermodynamically. Compared to the $RuSe_2$ bulk composition, this surface is rather Se-rich and has two additional Se atoms per surface unit cell. Again, at this phase separation line the close-packed (111) surface is not the most stable, but the more opened (100)-surface. This is certainly a consequence of Se preferentially occupying surface sites. On (100) this is much more sufficient than that on $RuSe_2$(111). Increasing the Ru chemical potential ($\Delta\mu_{Ru}$) leads to a successive depletion of Se from the surface, even resulting in a Ru-terminated surface [$RuSe_2$(111)-Conf. 4] for

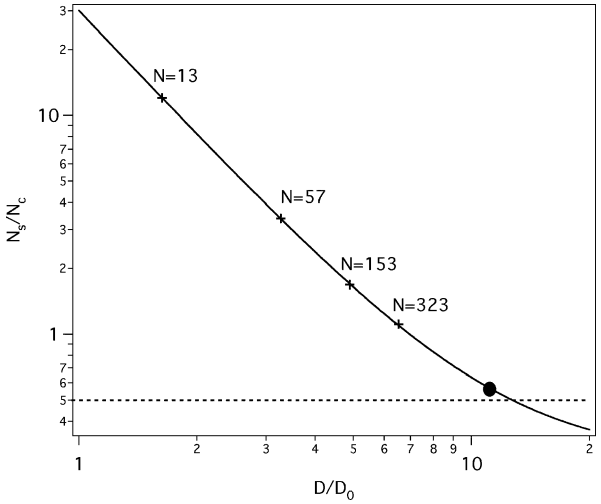

Figure 9. Ratio of the number of surface to core atoms, N_s/N_c, as a function of cluster diameter, D/D_0. The "magic-numbers" of *hcp* cluster are shown as crosses in the figure. D_0 is the interatomic distance (D_0 = 2.71 Å for Ru).

high values of $\Delta\mu_{Ru}$. This already indicates a preference for a Se-terminated surface even under conditions where the bulk compound should form. Interestingly, the phase diagram shows that when μ_{Ru} is increased the preferred surface orientation alternates between $RuSe_2(100)$ and $RuSe_2(111)$. $RuSe_2(110)$, which one would expect to have a lower surface free energy than $RuSe_2(100)$, plays only a minor role. Although among the bulk-terminated surfaces $RuSe_2(100)$ is the most stable (see horizontal lines in Figure 7), it seems that the presence of additional Se on the surfaces of $RuSe_2(111)$ increases their stability.

Finally, it should be remarked that the above considerations did not take any kinetic barrier into account, which might be involved in forming $RuSe_2$ bulk out of Ru bulk and Se bulk. As already mentioned above, we are now in the process of performing larger scale molecular dynamic (MD) simulations on the growing process itself. For this, all of the DFT calculations (structures and energies) described in the present paper were used to generate an accurate Ru/Se interaction.

Cluster-like Formation Dynamics during Pyrolysis. As shown in Figures 2 and 3−5, the evolution of the final catalyst particle nanostructure, under temperature-controlled conditions, depends on significant initial fragmentation of the heteronuclear cluster framework followed by preferential nucleation at ruthenium centers. From model calculations, we know that the relative intensity function will not be significantly modified by replacement of some surface Ru atoms by Se atoms, even if the Ru−Se distance is altered against the Ru−Ru distance.[4] After pyrolysis of the precursor molecule, only a single phase remains. This phase can be quantitatively attributed to a nanocrystalline phase of *hcp*-type. If the selenium atoms did not escape fugacious (which would only be partly possible, because the selenium reappears as $RuSe_2$ at high temperature), then we would have seen it because it cannot be overlooked, due to the fact that the scattering power of Se is about 60% of that of Ru; thus, selenium should contribute about 30% to the total intensity. This proves that Se must be incorporated into the *hcp* particles. There is no direct proof that Se is located at the nanoparticle surface. But there are two arguments that strongly support this thesis: (i) Se is insoluble in bulk ruthenium, and (ii) if Se would in fact show a solubility to Ru on a nanoscale, then we would expect a measurable change of the mean interatomic spacing, which is not observed.

According to Figure 2, the thermal decomposition process can be subdivided into three regions related to the time of treatment, namely, (*i*) 20−30 min (150−240 °C) breakdown of the carbonyl and formation of ruthenium clusters; (*ii*) 30−65 min (240−440 °C) slow growth of the preformed cluster by coalescense; and (*iii*) 65−80 min (440−500 °C) formation of a phase separation.

All of these processes describe the cluster evolution. The curve discontinuity, observed at $t = 30$ min, shows a sudden completion of the metallic cluster formation. As support, the dynamics leading to the formation of segregated core structures finds precedent in other bimetallic systems.[23] The insight, however, in this work is that chalcogen coordination takes place onto ruthenium surface atoms and that there is formation of a narrow size distribution in the nonsupported chalcogenide particles with a compositional distribution, of 2:1 [Ru/Se], in full agreement with previously reported works[3,4,10,11] on the catalyst synthesized in organic solvent.

Moreover, the spectrum taken at 430 °C (Figure 4) already indicated the beginning of the formation of pyrite-type domains. As a matter of fact, according to the fixed ratio of Ru/Se (2:1) given by the initial compound $Ru_4Se_2(CO)_{11}$, the proposed segregation of selenium to the surface of *hcp* clusters will go into a saturation with the increasing cluster size, as shown in Figure 9.

The number of surface atoms, N_s, related to the core atom number, N_c, is plotted versus the cluster diameter D for N = 13, 57, and 153. The extrapolated curve to $N_s/N_c = 0.5$ furnishes a critical cluster size of 3.4 nm. The circle in Figure 9 indicates the cluster size determined in Figure 5, at the beginning of the formation of pyrite $RuSe_2$. Further growth would lead to an excess of selenium onto the ruthenium surface, favoring pyrite formation. In full agreement with these considerations, the embryonic nucleation of pyrite $RuSe_2$ domains is observed at the cluster size of 3.1 nm; see Figures 4 and 5. Furthermore, as clearly shown by DFT calculations, the Ru−Se system evolves with the temperature up to a thermodynamically stable phase formation within a pyrite structure: $RuSe_2$. The latter is a low-band gap semiconductor (0.76 eV).[24] Summing up, the material dynamics takes place from a heteronuclear cluster compound to a semiconductor, crossing through a chemically stable selenium coordinated ruthenium core. This chemical phenomenon leading to a catalyst material, totally tolerant for the oxygen reduction reaction in the presence of methanol,[3] represents the bottom-up approach of ruthenium selenide Ru_xSe_y.[4] It also explains the catalytic activity nature of ruthenium-black's surface[25] modified with selenium and/or the ruthenium chemical-generated and further modified by selenium.[26]

Conclusions

In summary, nanodivided Ru_xSe_y cluster-like materials are derived from pyrolysis of a heteronuclear transition-metal complex compound. This phenomenon takes place between 200 and 240 °C. Under this condition, the chalcogen atoms organize preferentially on the surface of the core-formed agglomerated ruthenium atoms. The Ru_xSe_y represents a prior intermediate state before reaching a more stable compound with a pyrite structure. As a combination of DFT calculations and thermodynamic considerations indicate, even under conditions where $RuSe_2$ is the thermodynamically stable bulk phase, a Se-rich surface is preferred. If the two separated bulk phases (Ru bulk and Se bulk) are thermodynamically more stable, then Se might coordinate forming a thin selenide phase on the surface of a Ru particle.

Acknowledgment. N.A.V. expresses his thanks to the Alexander von Humboldt Stiftung and the Max-Planck-Society for funding his stay at the Fritz-Haber-Institut. T.J. greatly acknowledges support by the "Fonds der Chemischen Industrie" (VCI) and P.K. by the German Academic Exchange Service (DAAD). We are grateful to Dr. T. Lana-Villarreal for her help in the complex preparation.

References and Notes

(1) Alonso-Vante, N.; Tributsch, H. *Nature* **1986**, *323*, 431.
(2) Schmidt, T. J.; Paulus, U.; Gasteiger, H.; Alonso-Vante, N.; Behm, R. J. *J. Electrochem. Soc.* **2000**, *147*, 2620.
(3) Alonso-Vante, N. *In Handbook of Fuel Cells*; Vielstich, W., Lamm, A., Gasteiger, H., Eds.; John Wiley & Sons Ltd.: Chichester, U.K., 2003; Vol. *2*, Part 5, p 534.
(4) Dassenoy, F.; Vogel, W.; Alonso-Vante, N. *J. Phys. Chem. B* **2002**, *106*, 12152.
(5) Rodriguez, F. J.; Sebastian, P. *J. New Mater. Electrochem. Syst.* **1999**, *2*, 107.
(6) Alonso-Vante, N. *Fuel Cells* **2006**, *6*, 182.
(7) Johnson, B. F. G.; Layer, T. M.; Raithby, P. R.; Wong, W.-T. *J. Chem. Soc. Dalton Trans*. **1993**, 973.
(8) Gnutzmann, V.; Vogel, W. *J. Phys. Chem.* **1990**, *94*, 4991.
(9) Vogel, W. *Cryst. Res. Technol.* **1998**, *33*, 1141.
(10) Le Rhun, V.; Alonso-Vante, N. *J. New Mater. Electrochem. Syst.* **2000**, *2*, 475.
(11) Alonso-Vante, N. *In Catalysis and Electrocatalysis at Nanoparticle Surfaces*; Wieckowski, A., Savinova, E., Vayenas, C., Eds.: Marcel Dekker, Inc.: New York, 2003; p 931.
(12) Le Rhun, V. University of Poitiers, Ph.D. Thesis, 2001.
(13) Layer, T. M.; Lewis, J.; Martin, A.; Raithby, P. R.; Wong, W.-T. *J. Chem. Soc. Dalton Trans*. **1992**, 3411.
(14) Hartmann, M.; Imbiehl, R.; Vogel, W. *Catal. Lett.* **1994**, *28*, 373.
(15) Vogel, W.; Alonso-Vante, N. *J. Catal.* **2005**, *232*, 395.
(16) Schultz, P. A. Unpublished work. A description of the method is in the following: Feibelman, P. *J. Phys. Rev. B* **1987**, *35*, 2626.
(17) Verdozzi, C.; Schultz, P. A.; Wu, R.; Edwards, A. H.; Kioussis, N. *Phys. Rev. B* **2002**, *66*, 125408.
(18) Perdew, J. P.; Burke, K.; Ernzerhof, M. *Phys. Rev. Lett.* **1996**, *88*, 3865.
(19) Hamann, D. R. *Phys. Rev. B* **1989**, *40*, 2980.
(20) Louie, S. G.; Froyen, S.; Cohen, M. L. *Phys. Rev. B* **1982**, *26*, 1738.
(21) Blaha, P.; Schwarz, K.; Luitz, J. Computer code WIEN97, TU Wien, Austria, 1999.
(22) The small drop of the intensity before the dramatic increase can be explained by the breakdown of the carbonyl structure in the Bragg window at 21.4°, cf. Figure 2.
(23) Nashner, M. S.; Somerville, D. M.; Lane, P. D.; Adler, D. L.; Shapley, J. R.; Nuzzo, R. G. *J. Am. Chem. Soc.* **1996**, *118*, 12964.
(24) Vaterlaus, H. P.; Bichsel, R.; Levy, F.; Berger, H. *J. Phys. C: Solid State Phys.* **1985**, *18*, 6063.
(25) Cao, D.; Wieckowski, A.; Inukai, J.; Alonso-Vante, N. *J. Electrochem. Soc*, **2006**, *153*, A869.
(26) Zaikovskii, V. I.; Nagabhushana, K. S.; Kriventsov, V. V.; Loponov, K. N.; Cherepanova, S. V.; Kvon, R. I.; Boennemann, H.; Kochubey, D. I.; Savinova, E. R. *J. Phys. Chem. B* **2006**, *110*, 6881.